Uncooled detector development for space application

W. Rabaud*[a], M. Vilain[b], J. Meilhan[a], T. Garret[b],
G. Hopkinson[c], M. S. Bentley[d], S. Kraft[d], O. Legras[b], P. Castelein[a]

[a] CEA-LETI, MINATEC – 17, rue des Martyrs, 38054 Grenoble Cedex 9, France
[b] ULIS - BP 27 – 38113 Veurey-Voroize, France
[c] Surrey Satellite Technology Ltd, Rayleigh House,1 Bat & Ball Road, Sevenoaks, Kent, TN14 5LJ, UK
[d] cosine Research B.V., Niels Bohrweg 11, 2333 CA Leiden, The Netherlands

ABSTRACT

The European Space Agency (ESA) has committed to a multi-spacecraft Cornerstone mission to the planet Mercury. BepiColombo comprises two spacecraft, one of which (The Mercury Planetary Orbiter platform (MPO)) will contain remote sensing instruments for making measurements of the planet at wavelengths from the far infrared to γ-rays. The MERcury Thermal Infrared Spectrometer (MERTIS) measures spectral emittance from Mercury in the range from 7 to 14 μm to derive surface mineralogy. It will employ an uncooled IR focal plane array (IRFPA) at the heart of the spectrometer. Within this framework, the IRFPA has been developed from a 160 x 120 microbolometer array with a pixel pitch of 35 μm. This sensor is made from amorphous silicon, which yields a short thermal time constant as well as very low NETD. Specific attention has been paid to the fact that such detector has to operate in space environment. The paper will present the specific development under progress and the first results obtained to fulfil the MERTIS requirements in terms of performance, irradiative and mechanical environments.

Keywords: Mercury, Uncooled microbolometer, LWIR, amorphous silicon, space environment

1. INTRODUCTION

Uncooled infrared thermal detectors are now available for various applications, ranging from military to commercial purposes. Recent performance improvements, as well as the achievement of small pixel pitches, make these uncooled detectors good candidates for high resolution applications. Moreover they are of interest for space applications due to the cost savings they allow in terms of power consumption, mass, size and/or an easy thermal control [1].
One scientific goal of MERTIS instrument is to study the mineralogical composition of the surface of Mercury by measuring the spectral emittance of the planet in the 7-14 μm range, with high spatial and spectral resolution. The only possible candidate for the detector, in the thermal infrared region of interest, which can be used in a hot environment such as at Mercury, is the uncooled microbolometer technology, where no cooling is required [2]. In the frame of the MERTIS development, the UBBA project was initiated to develop such an IRFPA, and more specifically, to enhance its performance to fulfil the MERTIS requirements.
In this paper, we discuss the specification of the sensor necessary to meet the requirements of MERTIS. Following a brief description of the sensor design, we report on the development programme undertaken to produce a detector meeting these requirements. Finally, the results on the environmental tests are reported, including thermal vacuum, vibration and radiation tests of the sensors.

2. SENSOR SPECIFICATIONS

The technical requirements of the microbolometer array flow directly from the science and measurement requirements of MERTIS to achieve excellent science at Mercury. The MPO spacecraft will orbit Mercury in an eccentric orbit with a periherm of 400 km and an apoherm of 1500 km. MERTIS measures thermal infrared radiation emitted from the surface

Sensors and Systems for Space Applications II, edited by Richard T. Howard, Pejmun Motaghedi,
Proc. of SPIE Vol. 6958, 69580P, (2008) · 0277-786X/08/$18 · doi: 10.1117/12.777993

of Mercury, the magnitude of which varies greatly over an orbit; Mercury has the largest diurnal temperature variation of any planet in the Solar System, ranging from 100 K to 700 K. These factors results in an instrument whose behaviour varies considerably over time and this must be considered when deriving the optimal performance.

Spectral emissivity variations on the surface of Mercury, caused by mineralogy, result in varying spectral emittance. To measure this, MERTIS acts as a hyperspectral imager. A grating diffracts radiation of different wavelengths across the array in the spectral direction, whilst the optics images the surface of the planet in the spatial direction. Measurements in the thermal infrared can be made with either cooled or uncooled detectors. The former have higher sensitivity and fast response times, but require cryogenic cooling. This is often incompatible with the lifetime or mass, power and vibration requirements of a space mission. MERTIS is therefore based around an uncooled microbolometer, a thermal detector that responds to incident radiation by a change in pixel temperature.

In order to derive a specification for the microbolometer array, the properties of the MERTIS instrument (optical efficiency, IFOV etc.) the MPO (orbital height, period etc.) and a typical microbolometer (detector absorptivity, window transmission etc.) were modelled. In particular, the NETD was calculated to achieve an SNR of 100, and the required average NETD is 13mK for typical laboratory operation (300K, f/1). This is already quite demanding and is not achievable over the entire spectral wavelength, but pixel binning can be applied, particularly close to periherm when the ground pixel size is smaller than required, to achieve better results. The thermal response time of the device must also be matched to the ground speed of the spacecraft. At the most simplistic level the time constant must be short enough to acquire an image without smearing caused by spacecraft motion. The limiting thermal time constant is derived from the highest ground velocity at periherm. If the MTF is to be degraded by less than 20% then a time constant of <~26 ms is required. The following sections describe the development activities undertaken to produce a sensor that meets the required specifications.

3. SENSOR ARCHITECTURE

Figure 1 shows a schematic drawing of a microbolometer pixel. As a thermal sensor, the detection of the IR radiation is not immediate, but involves an absorbing layer and a thermometer. The absorbing layer converts the incoming IR radiation into a temperature rise that will be detected by the thermometer. The magnitude of this temperature rise is closely related to the thermal insulation of the absorbing layer. This is rather high due to the properties of the arms supporting the membrane. The main characteristic of the thermometer is the change of its electrical resistance with respect to its temperature, which is read by a Read-Out Integrated Circuit (ROIC).

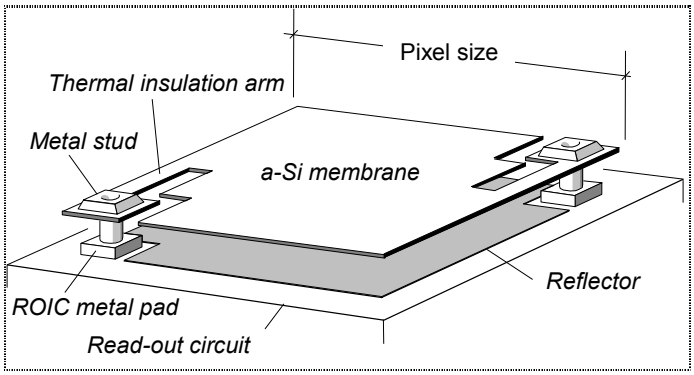

Figure 1. Schematic drawing of a micro-bolometer pixel.

4. PERFORMANCE ENHANCEMENT

The sensor developed for the MERTIS instrument is based on the 35 µm pixel pitch ULIS product, the UL02051, with a 160x120 format IRFPA. Figure 2 shows the UL02051 and Table 1 summarises its key parameters [3,4,5].

Figure 2. Packaging of the UL02051.

Array format	160 x 120
Pitch size	35 µm x 35 µm
Spectral response	8-14 µm
Fill factor	> 80%
Operability	> 99.9%
Power consumption	< 100 mW (without TEC)
Weight	< 10g
FPA temperature stabilization	integrated TEC
NETD (300K, f/1, 60Hz)	30 mK
Thermal time constant	7 msec

Table 1. Summarized parameters of the ULIS 35 µm.

In comparison to the state-of-the-art of the standard product, the performance required for this project implies a gain by a factor of 2 of the signal-to-noise ratio. To achieve this challenge, two technological improvements of the detector have been performed, and will be discussed here:

- increase the thermal insulation between the membrane and the ROIC, and
- development of a new membrane design.

Any change in the thermal conductance of the detector has a direct and linear effect on the NETD of the sensor (the sensor is defined as the detector plus the Read Out Integrated Circuit). The thermal conductance is controlled primarily by the arm design and, to a lesser degree, by radiative exchanges between the membrane and the surrounding environment. This radiative coupling is, in fact, an unwanted consequence of the membrane size. Instead of reducing the thicknesses of the arm that support the membrane, a more efficient improvement of the thermal conductance is achieved by reducing the arm width. As the equivalent thermal conductance of the radiative exchanges is one order of magnitude lower than the thermal conductance of the arm, the reduction of the arm width will act to first order in a linear way on the total thermal conductance. A new i-Line photo-lithography facility has been used to significantly reduce the arms width, and calculations have shown that this should lead to a gain of the signal-to-noise ratio of 1.6.

It should be stressed that reducing the arm width could have a negative effect on the mechanical stability of the membrane and therefore on the operability of the IRFPA. This point is addressed by environmental tests to investigate if the microbolometer strength is affected by this performance enhancement.

The design of the membrane is the second part of the detector improvement programme. The key changes are a new electrode design and, thanks to the arm width reduction, an increase in the width of the membrane. This first point reduces the noise of the thermometer by decreasing the local current density inside the amorphous silicon. The increase of the width of the membrane leads to an enhancement of the optical fill factor. Thus, the new design of the membrane should enhance the performance of the detector by a factor of 1.4. A total performed gain of 2 to 2.5 is then expected.

A new 35 µm uncooled IRFPA has been realized following these technological improvements. The ROIC of the sensor is the same as the standard product [5,6], and no particular care was taken regarding the space environment. The packaging is also identical, with the exception that the transmission of the infra-red (IR) window has been extended to a lower wavelength to fulfil the project specification.
Table 2 summarises the spectral properties of the new window.

window material	germanium
absolute transmittance below 5.8 µm	< 1%
5% transmittance cut-on wavelength (λc)	6.9 µm ± 1%
Cut-on slope	< 3%
average transmittance from 7.2 µm to 14 µm	> 90%
absolute transmittance from 7.2 µm to 14 µm	> 80%

Table 2. Specification of the spectral wavelength transmittance of the dedicated IR window.

The signal-to-noise ratio has been measured with a 300K TEC regulated focal plane temperature, and an equivalent f/1 number. The integrated capacitance of the TIA [5,6] is adjusted in order to have the best trade-off between the responsivity and the dynamic range, for nominal bias. The integration time has been increased up to 120 µsec, while keeping a frame time corresponding to 60 Hz, in order to extract the best signal-to-noise ratio.
Thanks to very low pixel-to-pixel electrical resistance dispersion, the noise and the responsivity have been measured at high bias voltage, and the required sensor performance extracted. Figure 3 and figure 4 show the typical noise, responsivity and temporal NETD at high bias voltage, and 303 K IRFPA temperature. The narrow statistical distribution of the responsivity measurements shows that the mechanical stability of the membrane is highly reliable. Moreover, the high biasing voltage leads to a responsivity that is, in the worst case, better than 50 mV/K, results in a temporal NETD below 15 mK. This new design of 35 µm microbolometer is of interest for ultra-high performance applications. Moreover, sensor performances analyses have been performed for different values of the bias voltage and are presented in Table 3. As expected, reducing the bias current through the sensitive µbolometer leads to an increase of the dynamic range, but also to a decrease of the signal-to-noise ratio as illustrated by the measured values of the temporal NETD.

biasing	temporal NETD (mK)	dynamic range (K)
low voltage	16	58
high voltage	11	19

Table 3. Summary of the temporal NETD and dynamic range measurements with respect to the biasing.

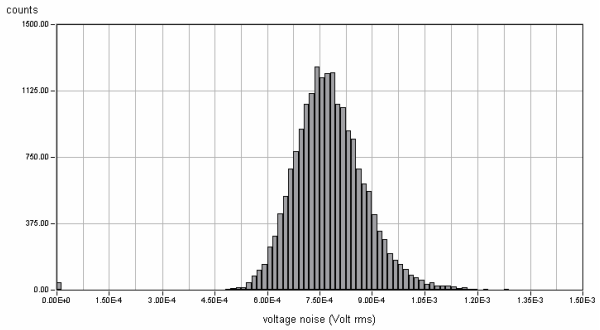

Figure 3a. Noise histogram: mean value = 780 µVrms

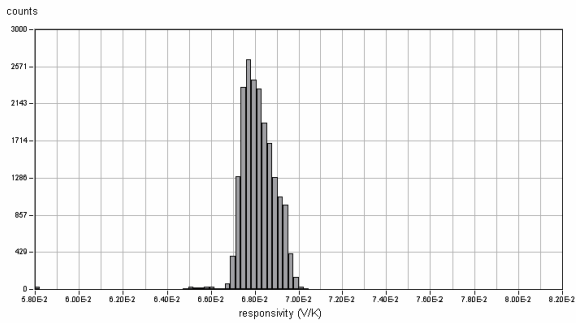

Figure 3b. Responsivity histogram: mean value= 68 mV/K

Figure 3. Noise and Responsivity histograms.

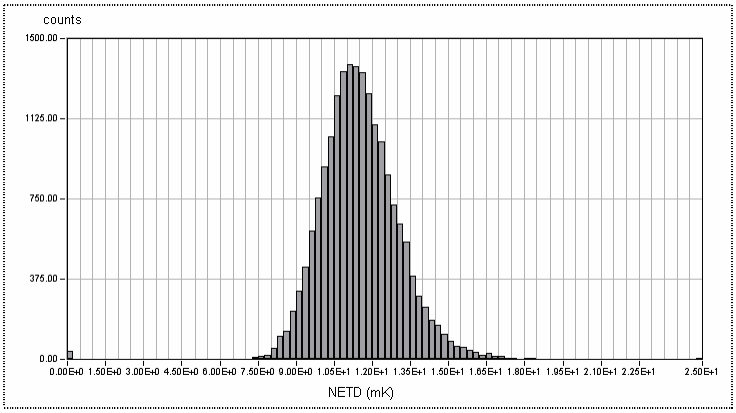

Figure 4. Temporal NETD measurements: mean value = 11 mK.

The measured values of the temporal NETD are ones of the best reported for the 35 µm uncooled µbolometers [5,6]. Moreover the performance gain obtained through these technological enhancements is close to a factor of 3, which is higher than expected. The best figure of merit that describes entirely the total performance of the uncooled micro-bolometer is the product of the temporal NETD by the thermal time constant as defined by Kohin *et al.* [7]. The figure of merit is then given by:

$$FOM = NETD \times \tau_{th} \quad [mK.msec]$$

The thermal time constant measured for the nominal thickness and for the high biasing options is 13.6 msec. Although this is a quite high value, this leads to a FOM of 150 mK.msec, what is one of the best reported value in the 35 µm pixel pitch family.

5. QUALIFICATION TEST AND RESULTS

One of the major development activities for MERTIS has been the definition and execution of a test and space evaluation plan for the microbolometer. Although a formal qualification of the device is not being performed, several examples of the enhanced sensor have been subjected to a variety of tests to ensure compatibility with the space environment. The BepiColombo spacecraft will endure a particularly hostile thermal and radiation environment during its cruise to the innermost planet and subsequent operations. These requirements, coupled with the usual space considerations of vacuum operation and launch vibration loads define a series of thermal, mechanical and radiation tests.

5.1. Thermal tests

Thermal tests are based on temperature cycling over a range chosen to simulate the extremes expected for the mission according to the requirements summarised in Table 4.

Parameter	**Value**
Minimum temperature	- 20 °C
Maximum temperature	+ 50 °C
Rate of change	dT / dt = 10° C / minute
Dwell Time	$T_E \geq$ 2 hours
Stabilisation criteria	$\Delta T / dt < 1°$ C / hour
Number of cycles	8 cycles

Table 4. Temperature cycling test parameters.

Since the inside of the microbolometer Dewar is evacuated, these tests were designed to examine the potential for performance degradation due to internal outgassing, or pixel failure due to thermal expansion and contraction. External outgassing phenomena of the package have been addressed with another specific test, in which empty bolometer packages are heated to the maximum temperature predicted for the sensor whilst under vacuum. No degradation of the detector has been seen after these thermal tests. The results of these tests are shown in Table 5.

Parameter	**Results**
Visual inspection	No damage before / after tests
Responsivity	Variation ≤ 0.5 %
NEDT	Variation ≤ 3 %
Operability	No variation

Table 5. Temperature cycling test results.

5.2. Mechanical environment

In order to ensure that the microbolometer survives the harsh mechanical environment of the launch phase, vibration tests have been performed. Sine and random vibrations are applied to the components at various levels. A low level resonance search is performed before and after each (more powerful) test in order to look for structural damages. The results confirm that the package and the assembly process will be strong enough to tolerate the launch loads. The complete sequence and the same levels are carried out for the Z, X and Y axes in turn (Table 6).
Acceleration measurements were performed with an accelerometer fixed onto the detector package as in Figure 5. Two reference sensors are located on the fixture, close to the devices. These are used by the control channel to ensure the shaker delivers the correct vibration levels. The results of the vibration tests are recorded in Table 7.

Item	**Frequency**	**Amplitude or level**	**Sweep rate** **No. of sweeps or duration**
Sine survey test	5 – 2 000 Hz	0.5 g	2 octave / min 1 sweep
Acceptance sine test	5 – 100 Hz 5 – 20 Hz 20 – 100 Hz	19.8 mm peak-to-peak 16 g	4 octave / min 1 sweep
Qualification sine test	5 – 100 Hz 5 – 20 Hz 20 – 100 Hz	30 mm peak-to-peak 24 g	2 octave / min 1 sweep
Acceptance random test	20 – 2 000 Hz 20 Hz 100 – 500 Hz 2 000 Hz	Overall level : 11.18 g_{rms} 0.005 g^2 / Hz 0.175 g^2 / Hz 0.005 g^2 / Hz	1 minute
Qualification random test	20 – 2 000 Hz 20 Hz 100 – 500 Hz 2 000 Hz	Overall level : 22.36 g_{rms} 0.005 g^2 / Hz 0.175 g^2 / Hz 0.005 g^2 / Hz	1 minute

Table 6. Resonance, sine and vibration levels carried out for Z, X and Y directions.

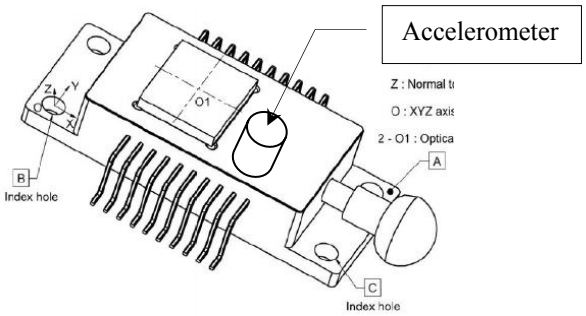

Figure 5. Mechanical reference and axis and accelerometer attachment.

Item	Results
Visual inspection	No damage before / after tests
Responsivity	Variation ≤ 0.5 %
NEDT	Variation ≤ 1 %
Operability	No variation
Resonance	No modification of the resonance frequency during tests

Table 7. Mechanical environmental test results.

6. RADIATIONS TESTS

Because of the proximity of the orbit to the sun, the BepiColombo radiation environment is significantly harsher than for many space missions. The main effect is expected to be due to solar protons which will give total ionizing dose (TID) damage in the CMOS readout integrated circuit (ROIC). The design dose, with a factor 2 design margin, is 100 krad (Si) behind 4 mm aluminium shielding and the effects were tested on 4 samples of the UL02051 ROIC using ^{60}Co gamma rays (2 devices were biased and 2 unbiased during the irradiation). The ESA ^{60}Co facility, in Noordwijk, The Netherlands was used, with a dose rate of 3.7 krad (Si) / hour. After the irradiation the devices were annealed unbiased at room temperature and then annealed at 100°C (for 168 hours) with the same bias as for irradiation.

With CMOS circuits it is also important to test for single event latch-up (SEL) effects caused by cosmic rays and this was done on 2 further samples of the ROIC, using heavy ions (the devices were de-lidded for this test because of the limited penetration depth, ~ 40 μm of beams available at ground-based accelerators). The heavy ion facility (HIF) at the Université Catholique de Louvain (UCL), Louvain la Neuve, Belgium was used to provide Xe, Kr and Ar ions with liner energy transfer (LET) in the range 14.1 to 55.9 MeV/mg/cm^2.

In detectors using crystalline semiconductors the solar protons will also lead to displacement damage and generation of defects, which may affect the performance (for example the dark current). Since, in this case, the detector element uses non-crystalline (amorphous) silicon, proton displacement damage is expected to be negligible (see, for example [8]). Nevertheless, a test (using 60 MeV protons) is planned - but (at the time of writing) has not yet been carried out. The test will be performed on 2 samples of the complete array (ROIC plus microbolometer) in the near future.

The ^{60}Co irradiations (and subsequent annealing) produced negligible change in clock switching voltages and the devices remained functional throughout. This indicates that there was no significant (i.e. less than 2 mV) change in the gate oxide flatband voltage (as is expected, since the gate oxides are very thin in modern CMOS foundry processes and so negligible charge is trapped because of irradiation). However, an increase in the analogue and digital Vdd bias supply currents was observed for the two devices biased during irradiation, as shown in figure 7. These currents decreased during subsequent anneals – so it is likely that the low dose rate space environment would produce only a small increase in supply current: of ~ 1mA for Vdd analog and ~ 2 mA for Vdd digital after 100 krad(Si). Note that increases in

leakage current are quite common in commercial-off-the-shelf CMOS devices because of the creation of parasitic leakage paths in thick field oxides used for isolation between transistors (see for example [9]).

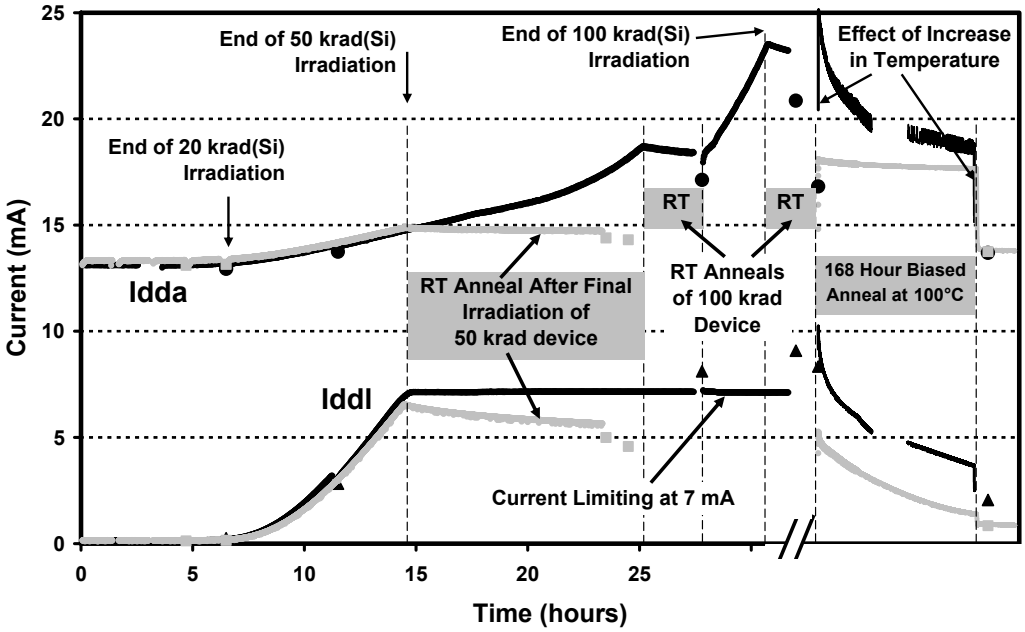

Figure 6. Bias currents for analogue (Idda) and digital (Iddl) supplies for the UL02051 multiplexers. Data are shown for the device irradiated up to 100 krad(Si) (black) and, 50 krad(Si) (grey). Periods of annealing are shown in grey (at room temperature, following irradiation and after 168 hours 100°C anneal for both devices). Data obtained with the devices taken out of the irradiation cell are shown by discrete symbols.

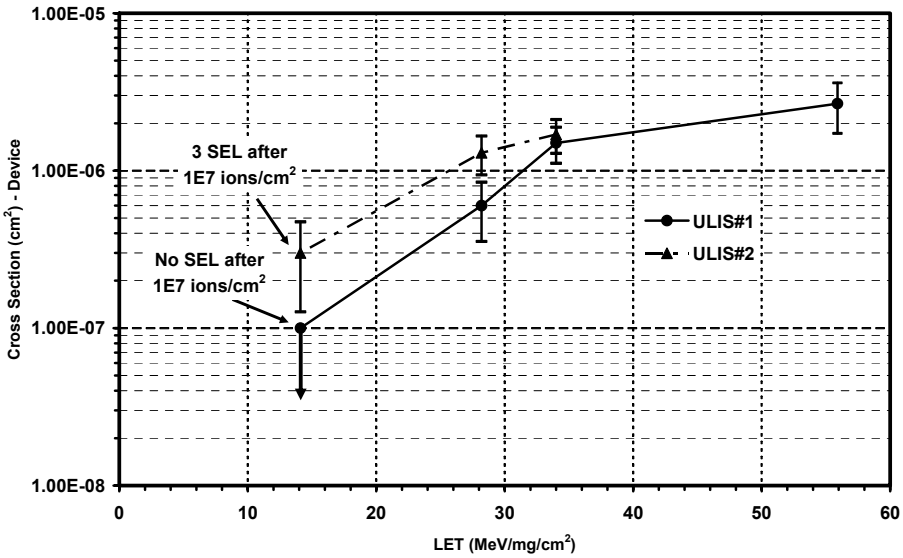

Figure 7. Measured latch-up cross-sections for the CMOS ROIC, the error bars are 1 sigma.

The CMOS ROIC was not designed to be radiation tolerant and latch up was seen at LETs above 14.1 MeV/mg/cm^2 as shown in figure 7. This gives the latch-up cross section (defined as the number of SEL Events divided by the ion fluence). These results indicate that latch-up protection circuits will be needed for space applications (to limit the supply current and thus prevent permanent damage). Note that the simple current limiting circuits used during the test were

successful in preventing device damage. The general conclusion of the tests conducted to date is that, although the devices were not specifically hardened to the space radiation environment, they will be suitable for demanding applications, such as BepiColombo - although latch-up protection will be needed.

7. CONCLUSION

In conclusion, the work performed in the UBBA project, in the framework of the MERTIS instrument development, has lead to a major improvement in the performance of the 35 µm pixel pitch microbolometer, with a measured temporal NETD of 11 mK. The new sensors have successfully passed thermal and vibration tests without any damage or performance degradation, and although these devices were not specifically hardened for the space radiation environment, they will be suitable for demanding space applications, such as BepiColombo.

ACKNOWLEDGEMENTS

The authors gratefully acknowledge the UBBA consortium members, Bruno Leone (ESA Technical Officer) for his support, and the MERTIS team from DLR for fruitful discussion. This work was funded by the European Space Agency (contract 19298/06/NL/PM).

REFERENCES

[1] J.J. Yon, G. Destefanis and E. Mottin, "Recent development in infrared technologies at LETI for earth observation", Proceedings of the SPIE, vol. **5570**, pp 525-536 (2004)
[2] MERTIS Instrument Interface Document – Part B, Draft C, rev. 0, (2006)
[3] UL02051 Technical Note, ULIS proprietary (2005)
[4] J.L. Tissot, A. Astier, J.P. Chatard, S. Tinnes, C. Trouilleau and J.J. Yon, "Low cost amorphous silicon based 160x120 uncooled microbolometer 2D array for high volume applications", Proceedings of the SPIE, vol. **5074**, pp 511-517 (2003)
[5] J.L. Tissot, A. Crastes, C. Trouilleau, B. Fieque and S. Tinnes, "Multipurpose high performance 160x120 uncooled IRFPA", Proceedings of the SPIE, vol. **5406**, pp 550-556 (2004)
[6] C. Trouilleau, A. Crastes, O. Legras, J.L. Tissot and J.P. Chatard, "35 µm pitch at ULIS, a breakthrough", Proceedings of the SPIE, vol. **5783**, pp 578-585 (2005)
[7] M. Kohin and N. Butler, "Performance limits of uncooled VOx microbolometer focal plane arrays", Proceedings of the SPIE, vol. **5406**, pp 447-453 (2004)
[8] N. Kishimoto, H. Amekura, K. Kono and C. G. Lee, "Radiation resistance of amorphous silicon in optoelectronic properties under proton bombardment", J. Nuclear Materials, vol. **258-263**, pp. 1908-1913 (1998)
[9] T. R. Oldham and F. B.McLean, "Total ionizing dose effects in MOS oxides and devices", IEEE Trans. Nucl. Sci., vol. **50(3)**, pp. 483-499 (June 2003)